

## Article

# Layered Perovskites $\text{BaM}_2\text{In}_2\text{O}_7$ ( $M = \text{La}, \text{Nd}$ ): From the Structure to the Ionic ( $\text{O}^{2-}, \text{H}^+$ ) Conductivity

Nataliia Tarasova <sup>\*</sup> , Anzhelika Galisheva, Irina Animitsa , Ksenia Belova , Anastasia Egorova , Ekaterina Abakumova and Dmitry Medvedev 

Institute of High Temperature Electrochemistry of the Ural Branch of the Russian Academy of Sciences, 620066 Ekaterinburg, Russia; a.o.galisheva@urfu.ru (A.G.); irina.animitsa@urfu.ru (I.A.); ksenia.belova@urfu.ru (K.B.); oav-hn@yandex.ru (A.E.); e.v.abakumova@urfu.ru (E.A.); dmitrymedv@mail.ru (D.M.)

\* Correspondence: natalia.tarasova@urfu.ru

**Abstract:** The design of new oxide compounds that can be used as oxygen- or proton-conducting electrolytes for solid oxide fuel cells is actively in progress. Despite the intensive research activities regarding electrolytes with perovskite/fluorite structures, the search for other structural alternatives is of paramount importance. In this study we focus on a novel material with significantly improved properties for the electrochemical purposes. The two-layered  $\text{BaNd}_2\text{In}_2\text{O}_7$  perovskite with a Ruddlesden–Popper structure was investigated as a protonic conductor for the first time. In detail, its local structure, water uptake, and the ionic ( $\text{O}^{2-}, \text{H}^+$ ) conductivity were comprehensively studied. The nature of rare-earth elements ( $M = \text{La}, \text{Nd}$ ) in the structure of  $\text{BaM}_2\text{In}_2\text{O}_7$  on the structural and transport properties was revealed. The presented analysis showed that the composition of  $\text{BaNd}_2\text{In}_2\text{O}_7$  is nearly pure proton conductor below 350 °C. This work opens up a new way in the design of protonic conductors with double-layered perovskite structure.

**Keywords:**  $\text{BaLa}_2\text{In}_2\text{O}_7$ ;  $\text{BaNd}_2\text{In}_2\text{O}_7$ ; layered perovskite; Ruddlesden–Popper structure; water uptake; oxygen-ion conductivity; protonic conductivity



**Citation:** Tarasova, N.; Galisheva, A.; Animitsa, I.; Belova, K.; Egorova, A.; Abakumova, E.; Medvedev, D. Layered Perovskites  $\text{BaM}_2\text{In}_2\text{O}_7$  ( $M = \text{La}, \text{Nd}$ ): From the Structure to the Ionic ( $\text{O}^{2-}, \text{H}^+$ ) Conductivity. *Materials* **2022**, *15*, 3488. <https://doi.org/10.3390/ma15103488>

Academic Editor:  
Alessandro Dell'Era

Received: 15 April 2022

Accepted: 11 May 2022

Published: 12 May 2022

**Publisher's Note:** MDPI stays neutral with regard to jurisdictional claims in published maps and institutional affiliations.



**Copyright:** © 2022 by the authors. Licensee MDPI, Basel, Switzerland. This article is an open access article distributed under the terms and conditions of the Creative Commons Attribution (CC BY) license (<https://creativecommons.org/licenses/by/4.0/>).

## 1. Introduction

The materials with layered perovskite-related structures have many various applications due to their different physical-chemical properties. These properties are dependent on the nature of ions in the crystal lattice. The structure of the compositions with the general formula  $\text{AA}'_2\text{B}_2\text{O}_7$  or  $\text{AO}(\text{A}'\text{BO}_3)_2$  can be described as the block-layered Ruddlesden–Popper (RP) structure where blocks consisting of two perovskite octahedra  $\text{A}'\text{BO}_3$  alternate with the salt AO layers [1]. The sum of charges of the cations in the A/A'- and B-sublattices can be obtained by the different variations such as +4 and +10, +6 and +8, and +8 and +6 (Figure 1). The total charge +4 in the A/A'-sublattice is typical for photocatalysts  $\text{A}_2\text{A}'\text{Ta}_2\text{O}_7$  where A is the hydrogen or alkali metal and A' is the alkali-earth metal [2–4]. The phosphors such as  $\text{Sr}_3\text{Sn}_2\text{O}_7:\text{Eu}^{3+}$  [5] and  $\text{Sr}_3\text{Ti}_2\text{O}_7:\text{Eu}^{3+}$  [6] have total charge +6 and +8 in the A- and B-sublattices, respectively. For the magnetic  $\text{A}^{\text{II}}\text{Ln}_2\text{Mn}_2\text{O}_7$  [7–12] and cathode  $\text{A}^{\text{II}}\text{Ln}_2\text{MM}'\text{O}_7$  [13–16] materials the sum of cationic charges can be written as +8 and +6, where  $\text{A}^{\text{II}}$  is the alkali-earth metal, Ln is the lanthanide, M and M' are metals with variable oxidation state such as Mn, Fe, Co, or Ni. In the case of the presence in the B-sublattice the metal with constant oxidation state such as indium, the chemical properties become completely different despite the same +8/+6 sum of cationic charges. As it was shown recently [17], the composition  $\text{BaLa}_2\text{In}_2\text{O}_7$  demonstrates nearly pure protonic transport under wet air and low temperatures and this phase can be potentially considered as the electrolytic material for the solid oxide fuel cell; therefore, the development of new materials with improvement properties is very relevant today [18–26].

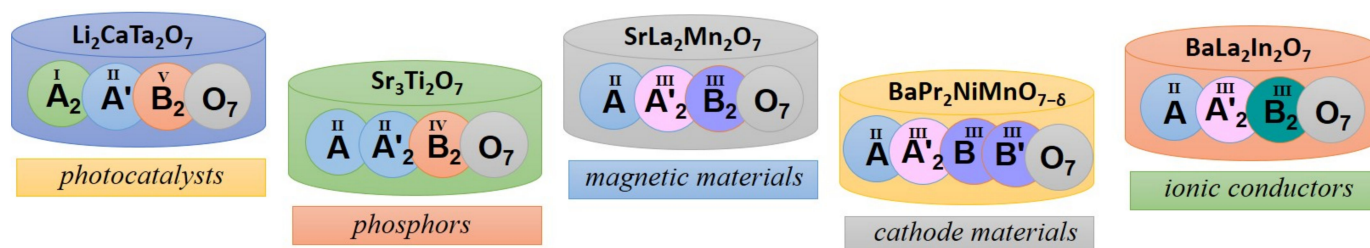


**Figure 1.** The overview of materials with a double-layered Ruddlesden–Popper structure.

The structure of the compounds  $\text{BaM}_2\text{In}_2\text{O}_7$  ( $M = \text{La}, \text{Nd}$ ) was described earlier by Titov et al. [27] and Raveau et al. [28]. It was shown that these phases belong to the RP structure  $\text{AO}(\text{A}'\text{BO}_3)_n$  where  $n = 2$ . The compositions with monolayered ( $n = 1$ ) RP structure in the system  $\text{Ba-Ln-In-O}$  are exist also. The complex oxides  $\text{BaNdInO}_4$  [29–34] and  $\text{BaLaInO}_4$  [35–41] and doped compositions based on it are mixed ionic or protonic conductors depending on the water partial pressure in the atmosphere and temperature. At the same time, in the row  $\text{BaLaInO}_4$ — $\text{BaNdInO}_4$  the ionic conductivity increased. Based on this, it can be predicted the same dependency in the row  $\text{BaLa}_2\text{In}_2\text{O}_7$ — $\text{BaNd}_2\text{In}_2\text{O}_7$ . From this point of view, the phase  $\text{BaNd}_2\text{In}_2\text{O}_7$  is of interest for studying their physicochemical properties.

In this paper, the local structure, water uptake, and the ionic ( $\text{O}^{2-}$ ,  $\text{H}^+$ ) transport in the complex oxide  $\text{BaNd}_2\text{In}_2\text{O}_7$  were investigated for the first time. It was shown that this material can be considered as the promising matrix compositions for development of novel high-conductive protonic electrolytes with PR structure.

## 2. Materials and Methods

The complex oxides  $\text{BaNd}_2\text{In}_2\text{O}_7$  and  $\text{BaLa}_2\text{In}_2\text{O}_7$  were obtained by the method of solid-state synthesis. The powder initial materials  $\text{BaCO}_3$ ,  $\text{La}_2\text{O}_3$ ,  $\text{Nd}_2\text{O}_3$ , and  $\text{In}_2\text{O}_3$  were previously dried, weighed, and mixed in stoichiometric quantities. The milling of powders was made in agate mortar. The compositions were calcined at 800, 900, 1000, 1100, 1200, and 1300 °C for 24 h at air, intermediate grindings were made for every following heating step.

The X-ray diffraction studies were made by the Bruker Advance D8 Cu  $K_\alpha$  diffractometer (Billerica, MA, USA) with a step of  $0.01^\circ$  and at a scanning rate of  $0.5^\circ/\text{min}$ . The local structure of the samples was investigated by the WiTec Alpha 300 AR Raman microscopy system (objective lens, blue laser, Ulm, Germany). The morphology and chemical composition of the samples were studied using a scanning electron microscope Phenom ProX Desktop (SEM) (Waltham, MA, USA) integrated with energy-dispersive X-ray diffraction (EDS) detector.

The Perkin Elmer Pyris 1 TGA thermogravimetric analyzer (London, UK) was used for the investigation of thermal behavior of the hydrated phase. The heating of initially hydrated samples was made at the temperature range of 40–1100 °C with speed of  $10^\circ\text{C}/\text{min}$  under a flow of dry Ar. The hydrated samples were obtained at slow cooling from 1100 to 150 °C ( $1^\circ\text{C}/\text{min}$ ) under a flow of wet Ar (99.999% purity,  $p_{\text{H}_2\text{O}} = 2 \times 10^{-2}$  atm). Ar atmosphere was used to avoid any carbonization of the samples.

The electrical conductivity was measured on the pressed cylindrical pellets using impedance spectroscopy method. The impedance spectrometer Z-1000P (Elins, RF, Uppsala, Sweden) with the frequency range of 1– $10^6$  Hz was used. The dependencies of conductivities vs. temperature were obtained in the temperature range of 200–1000 °C (step 10–20 °C,  $1^\circ/\text{min}$  cooling rate). All electrochemical investigations were performed under dry and wet air or Ar. The dry gas was produced by circulating the gas through  $\text{P}_2\text{O}_5$  ( $p_{\text{H}_2\text{O}} = 3.5 \times 10^{-5}$  atm). The wet gas was obtained by bubbling the gas at room temperature first through distilled water and then through saturated solution of KBr ( $p_{\text{H}_2\text{O}} = 2 \times 10^{-2}$  atm). The humidity of the gas was controlled by a Honeywell HIH-3610  $\text{H}_2\text{O}$  sensor. The dependencies of conductivities vs. partial oxygen pressures  $p_{\text{O}_2}$  were obtained by using the electrochemical method for producing different  $p_{\text{O}_2}$  with oxygen

pump (and sensor) from Y-stabilized ZrO<sub>2</sub> ceramic. The values of the resistance were recorded after 3–5 h of equilibrium.

### 3. Results

#### 3.1. Material Characterization

The powder samples BaM<sub>2</sub>In<sub>2</sub>O<sub>7</sub> (M = La, Nd) were investigated using X-ray diffraction analysis. The both compositions were single phase, and they are indexed in the tetragonal symmetry (space group *P4<sub>2</sub>/mmm*) (Figure 2a). The lattice and structural parameters were in good agreement with previously reported by Titov et al. and Raveau et al. data [27,28] (Table 1).

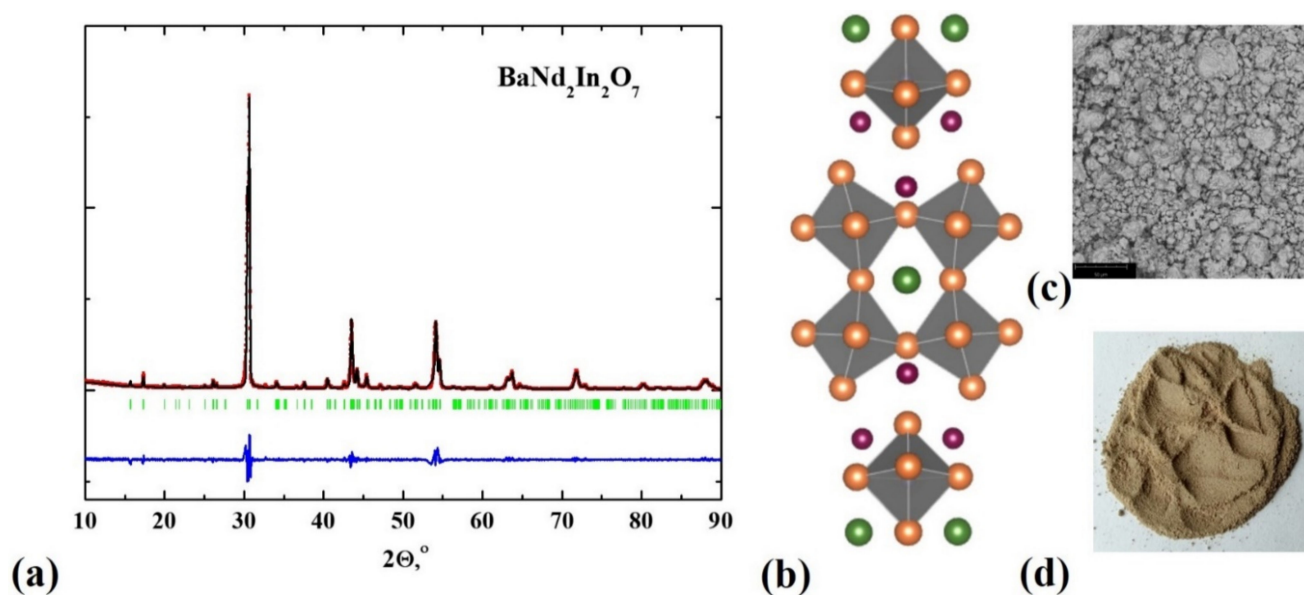


**Figure 2.** Materials characterization of the BaNd<sub>2</sub>In<sub>2</sub>O<sub>7</sub> compound: XRD patterns (a), image of double-layered RP crystal structure (b), SEM-image (c), and image of powder sample (d).

**Table 1.** Unit cell parameters and volume of the BaNd<sub>2</sub>In<sub>2</sub>O<sub>7</sub> and BaLa<sub>2</sub>In<sub>2</sub>O<sub>7</sub> compounds.

Composition	Unit Cell Parameters	This Work	Titov et al. [27]	Raveau et al. [28]
BaNd <sub>2</sub> In <sub>2</sub> O <sub>7</sub>	a, Å	5.8916(9)	5.8969(8)	5.8940(3)
	c, Å	20.469(0)	20.439(3)	20.467(1)
	V, Å <sup>3</sup>	710.52	710.76	711.02
BaLa <sub>2</sub> In <sub>2</sub> O <sub>7</sub>	a, Å	5.914(9)	5.915(2)	5.9141(3)
	c, Å	20.846(5)	20.861(1)	20.831(2)
	V, Å <sup>3</sup>	729.34	729.92	729.73

The morphology of the samples was investigated using scanning electron microscopy (SEM) method. The size of the grains was ~5–10 μm; the agglomerates with the size up to 30–50 μm were also found (Figure 2c). Figure 2d represents the image of the powder sample BaNd<sub>2</sub>In<sub>2</sub>O<sub>7</sub>. The chemical composition was checked via the energy-dispersive (EDS) analysis. The good agreement between theoretical and experimental values of chemical composition was proved by the energy-dispersive (EDS) analysis performed on the polished cleavages of the ceramic samples (Table 2).

**Table 2.** The average metal ratios determined by EDS analysis for the  $\text{BaNd}_2\text{In}_2\text{O}_7$  and  $\text{BaLa}_2\text{In}_2\text{O}_7$  compounds (theoretical values are given in the brackets).

Element	Content of the Elements, Atomic %	
	$\text{BaNd}_2\text{In}_2\text{O}_7$	$\text{BaLa}_2\text{In}_2\text{O}_7$
Ba	8.81 (8.33)	8.42 (8.33)
La/Nd	16.23 (16.67)	16.37 (16.67)
In	16.95 (16.67)	16.71 (16.67)
O	58.01 (58.33)	58.50 (58.33)

### 3.2. Oxygen-Ionic Conductivity

The conductivity measurements were made using the impedance spectroscopy method. As an example, the typical Nyquist plot is presented in Figure 3. The experimental data are showed by the blue symbols, and the fitting of the spectra (ZView software) is represented by the red line. According to the spectra, two different electrochemical processes can be defined. The semicircle started from the zero coordinates corresponds to the bulk resistance with the capacity  $\sim 10^{-12}$  F. The small semicircle in the low-frequency region is characterized by the capacity  $\sim 10^{-10}$  F and it corresponds to the resistance of the grain boundaries. It should be noted what the Nyquist plots for the monolayer composition  $\text{BaNdInO}_4$  described by Yang et al. [33] was characterized by the same shape. For the calculation of electrical conductivity, the bulk resistance values were used.

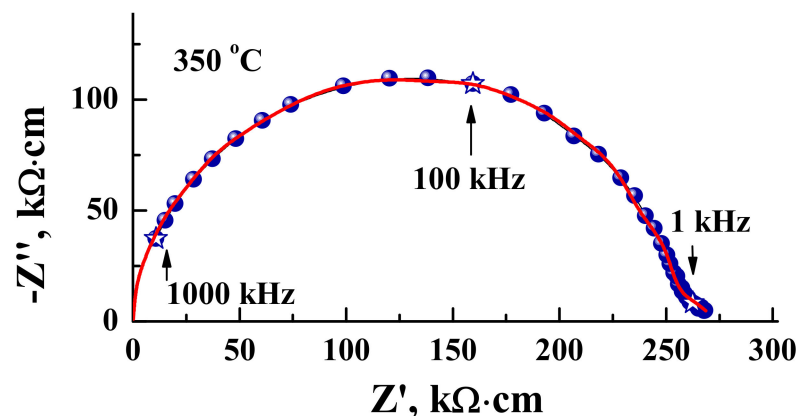


**Figure 3.** The Nyquist-plot for the  $\text{BaNd}_2\text{In}_2\text{O}_7$  ceramic material obtained at 350 °C under dry air.

The temperature dependencies of conductivity obtained under dry condition ( $p_{\text{H}_2\text{O}} = 3.5 \times 10^{-5}$  atm) are presented in Figure 4a. As can be seen, the conductivity values for the composition  $\text{BaNd}_2\text{In}_2\text{O}_7$  are higher than for the  $\text{BaLa}_2\text{In}_2\text{O}_7$  [17]. The increase in the conductivity is about one order of magnitude under dry air condition. In the dry Ar, this difference is up to 1.2 order of magnitude. The dependencies of conductivity vs. oxygen partial pressure under dry condition are presented in Figure 4b. The right part of the curves (in the  $p_{\text{O}_2}$  range of  $10^{-5}$ –0.21 atm) had a positive slope which corresponded to the electronic conductivity (p-type). The conductivity values are independent on the oxygen partial pressure below  $10^{-5}$  atm, and this region belongs to the electrolytic area. It should be noted, that conductivity values obtained from “ $\sigma-1/T$ ” dependencies (orange symbols, Figure 4b) well correlated with the values obtained from “ $\sigma-p_{\text{O}_2}$ ” dependencies (blue symbols, Figure 4b). Based on this, the conductivity values obtained under dry Ar can be considered as the oxygen-ionic conductivity values. Consequently, the oxygen-ionic transport number  $t_{\text{O}^{2-}}$  can be calculated as:

$$t_{\text{O}^{2-}} = \frac{\sigma_{\text{O}^{2-}}}{\sigma_{\text{tot}}} = \frac{\sigma_{\text{Ar}}}{\sigma_{\text{air}}} \quad (1)$$

The oxygen-ionic transport numbers for the compounds  $\text{BaLa}_2\text{In}_2\text{O}_7$  and  $\text{BaNd}_2\text{In}_2\text{O}_7$  were around 20% and 50% correspondingly, i.e., the share of oxygen transport was bigger for the Nd-containing sample. For the explanation of this fact, the nature of oxygen transport should be considered.

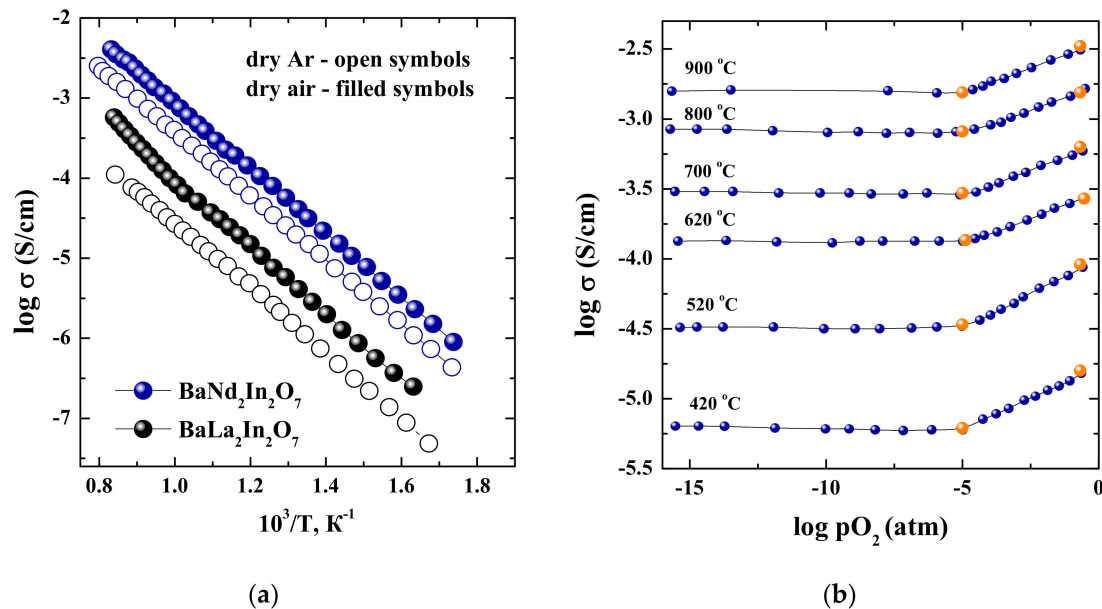


**Figure 4.** Temperature dependencies of conductivity for  $\text{BaNd}_2\text{In}_2\text{O}_7$  (blue symbols) and  $\text{BaLa}_2\text{In}_2\text{O}_7$  (black symbols) [17] obtained for dry Ar (open symbols) and dry air (filled symbols) (a); oxygen partial pressure dependencies of the total conductivity values for the  $\text{BaNd}_2\text{In}_2\text{O}_7$  sample at dry conditions (blue symbols) and conductivity values from  $\sigma-10^3/T$  dependencies in dry air and Ar (orange symbols) (b).

The layered RP-structure  $\text{BaM}_2\text{In}_2\text{O}_7$  with  $n = 2$  consists of alternating salt layers and perovskite blocks where two octahedra  $[\text{InO}_6]$  layers are connected to each other by vertices (Figure 2b). The barium atoms are located in the perovskite blocks in the space between  $[\text{InO}_6]$  octahedra and they have 12 coordination numbers. The atoms of rare earth elements (La and Nd) are placed in the salt layers and they are characterized by a coordination number of 9. The increase in the coordination number of La or Nd atoms up to 12 is theoretically possible, and this process can be described in terms of anti-Frenkel disordering:



where  $\text{O}_\text{i}^{\prime\prime}$  is the oxygen atom in the interstitial position;  $\text{V}_\text{O}^{\bullet\bullet}$  is the oxygen vacancy. In this case, the coordination number of La/Nd atoms increases, and the coordination number of In atoms decreases. Returning to the experimental data, we can say that in the row  $\text{BaLa}_2\text{In}_2\text{O}_7$ – $\text{BaNd}_2\text{In}_2\text{O}_7$  not only total conductivity increases, but the share of oxygen-ionic transport increases also. Consequently, the different nature of rare earth elements (La or Nd) in the crystal lattice of layered perovskite  $\text{BaM}_2\text{In}_2\text{O}_7$  leads to the changes in the degree of disordering and the change in the local structure.

The local structure of compounds  $\text{BaLa}_2\text{In}_2\text{O}_7$  and  $\text{BaNd}_2\text{In}_2\text{O}_7$  was investigated using Raman spectroscopy. The results of the deconvolution of obtained Raman spectra are presented in Figure 5. The region of low wavenumbers ( $120$ – $200 \text{ cm}^{-1}$ ) is represented by the bending and stretching vibrations of polyhedral, containing alkali earth and rare earth metals [40–43], i.e.,  $[\text{BaO}_{12}]$ ,  $[\text{LaO}_9]$ , and  $[\text{NdO}_9]$ . In this region, the modes  $\nu_1$ ,  $\nu_2$ ,  $\nu_3$ , and  $\nu_4$  are observed (Table 3). They can be ascribed to the M–O stretching and O–M–O bending vibrations where M is the Ba, La, or Nd. For the composition  $\text{BaNd}_2\text{In}_2\text{O}_7$  the red shift (i.e., shift towards lower wavenumbers) is observed. In general, the red shift indicates the

increase in the part of bond lengths M–O. However, due to the presence of several cations in the A- and A'-sublattices of  $AA_2B_2O_7$ , the correct interpretation of this shift is difficult.

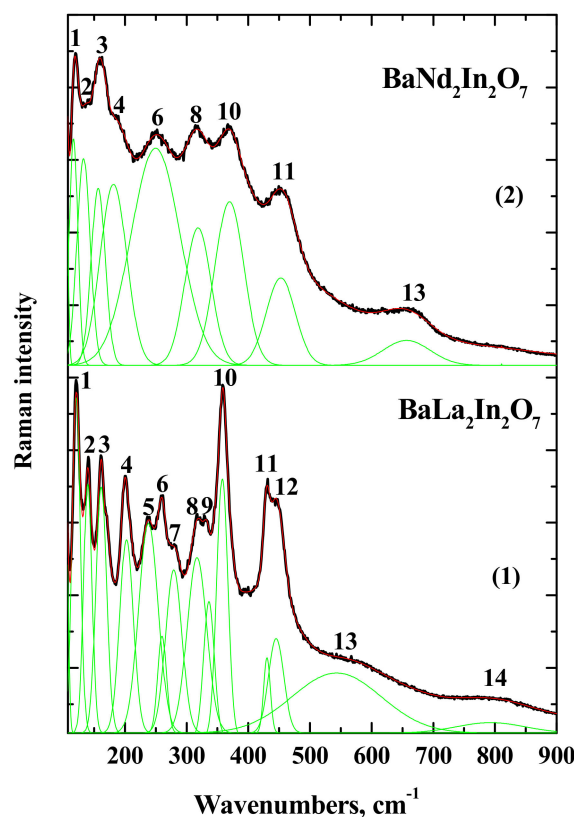


Figure 5. Raman spectra of the  $BaLa_2In_2O_7$  (1) and  $BaNd_2In_2O_7$  (2) compounds.

Table 3. Wavenumbers ( $cm^{-1}$ ) of Raman bands for the  $BaNd_2In_2O_7$  and  $BaLa_2In_2O_7$  compounds.

No of Band	$BaLa_2In_2O_7$	$BaNd_2In_2O_7$
1	120	118
2	140	133
3	161	157
4	203	181
5	237	-
6	260	250
7	279	-
8	316	319
9	336	-
10	358	370
11	430	453
12	445	-
13	545	660
14	800	-

The region of mid and high wavenumbers (higher than  $200\text{ cm}^{-1}$ ) contains the tilting/bending and stretching vibrations of In-contained polyhedra. The band  $\nu_5, \nu_6, \nu_7, \nu_8,$  and  $\nu_9$  can be described as the tilting/bending vibration of polyhedra  $[InO_6]$ . These five bands are well visible in the spectrum of  $BaLa_2In_2O_7$ , while the spectrum of  $BaNd_2In_2O_7$  contains two ( $\nu_6$  and  $\nu_8$ ) bands only. It can be said, that  $\nu_6$  and  $\nu_8$  bands in the spectrum of  $BaNd_2In_2O_7$  degenerate to the  $\nu_5, \nu_6, \nu_7, \nu_8,$  and  $\nu_9$  bands in the spectrum of  $BaLa_2In_2O_7$  correspondingly. Based on this, it can be assumed that tilting of In-containing octahedra decreases in the row  $BaLa_2In_2O_7$ – $BaNd_2In_2O_7$ . According to the structural data reported by Titov et al. [27], the degree of deformation of  $[InO_6]$  polyhedra decreases and the In–O–In

angle is approaching to  $180^\circ$  from  $\text{BaLa}_2\text{In}_2\text{O}_7$  to  $\text{BaNd}_2\text{In}_2\text{O}_7$ . The band  $\nu_{14}$  registered in the spectrum of  $\text{BaLa}_2\text{In}_2\text{O}_7$  can be ascribed to the repulsion between the  $\text{Ba}^{2+}/\text{La}^{3+}(\text{Nd}^{3+})$  ions and apical oxygen ions in compressed In-contained polyhedra [44]. The decrease in the tilting of In-contained polyhedra in the row  $\text{BaLa}_2\text{In}_2\text{O}_7\text{--BaNd}_2\text{In}_2\text{O}_7$  can lead to the disappearance of this band in the spectrum of  $\text{BaNd}_2\text{In}_2\text{O}_7$ .

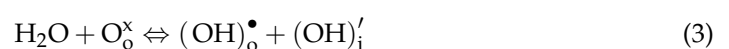
The stretching vibrations of In-contained polyhedra locate in the higher wavenumbers. Based on the analysis of Raman spectra of monolayer RP-composition  $\text{BaLaInO}_4$  [40,41], the stretching vibrations of In–O bonds should be appeared around  $400\text{ cm}^{-1}$ . At the same time, the comparable analysis of Raman spectra of RP homologous series  $\text{Sr}_{n+1}\text{Ti}_n\text{O}_{3n+1}$  [45] and  $\text{Sr}_{n+1}\text{Ru}_n\text{O}_{3n+1}$  [46] showed that the signal corresponded to the M–O stretching vibrations for monolayer compositions transforms into two signals with lower and higher wavenumbers in the spectra of double-layered RP-compositions. Thus, the bands  $\nu_{10}$ ,  $\nu_{11}$ , and  $\nu_{12}$  can be attributed to stretching vibrations of In–O bonds. As can be seen, the blue shift (i.e., shift towards higher wavenumbers) of  $\nu_{10}$  and  $\nu_{11}$  bands is observed for  $\text{BaNd}_2\text{In}_2\text{O}_7$  composition compared with  $\text{BaLa}_2\text{In}_2\text{O}_7$  composition. This shift indicates the decrease in some In–O bond lengths.

The local distortion of the crystal lattice due to anti-Frenkel disordering (Equation (2)) can lead to the formation of oxygen vacancies in the In-contained polyhedra, and the polyhedra with lower coordination number [ $\text{InO}_{6-x}$ ] appear in the structure. At the same time, the formation of oxygen interstitial leads to the increase in the coordination number of some cations. Most reasonable candidate for this is the rare earth element because both La and Nd have a coordination number of 9, and they can increase it up to 12 theoretically. Thus, the formation of polyhedra [ $\text{La}(\text{Nd})\text{O}_{9+x}$ ] is possible. It is obvious that the decrease in the coordination number of metal leads to the decrease in some part of metal–oxygen bond length, and the signal with higher wavenumber should appear in the spectrum, what was observed for the composition  $\text{BaLaInO}_4$  [40,41]. We can assume that the signal  $\nu_{13}$  in the spectra of  $\text{BaNd}_2\text{In}_2\text{O}_7$  and  $\text{BaLa}_2\text{In}_2\text{O}_7$  can be attributed to the motion of In-contained polyhedra with a lower coordination number.

The blue shift of  $\nu_{13}$  band for the  $\text{BaNd}_2\text{In}_2\text{O}_7$  indicates that the decrease in the part of In–O bond lengths is more pronounced. Thus, we can assume that for the Nd-contained compound the formation of oxygen vacancies due to local distortion is more favorable in comparison with  $\text{BaLa}_2\text{In}_2\text{O}_7$  composition. This result is in good agreement with the crystallographic point of view, because the lower coordination number is more favorable for the ion with smaller ionic radius ( $r_{\text{Nd}^{3+}} = 1.163\text{ \AA}$ ,  $r_{\text{La}^{3+}} = 1.216\text{ \AA}$  [47]). In this way, the concentration of oxygen defects (oxygen vacancies and oxygen interstitial) should be higher in the composition  $\text{BaNd}_2\text{In}_2\text{O}_7$  compared with the composition  $\text{BaLa}_2\text{In}_2\text{O}_7$ , and the share of oxygen-ionic conductivity should be higher also. Returning to obtained experimental data, we can say, that the results of electrical measurements are well correlated with the Raman spectroscopy results. The electrical conductivity and the share of oxygen-ionic transport increased in the row  $\text{BaLa}_2\text{In}_2\text{O}_7\text{--BaNd}_2\text{In}_2\text{O}_7$ .

### 3.3. Protonic Conductivity

The possibility of water uptake for the compounds with PR-structure is provided by the opportunity of the cations increase their coordination numbers. For the composition  $\text{BaM}_2\text{In}_2\text{O}_7$  the hydration may be due to increase in the coordination number of atoms M and the formation of polyhedra [ $\text{MO}_8(\text{OH})_2$ ]. This process can be described by the quasi-chemical equation as:



where  $(\text{OH})_o^\bullet$  is the hydroxyl group in the regular oxygen position;  $(\text{OH})_i'$  is the hydroxyl group located in the interlayer space. However, in the case of the presence oxygen vacancies in the structure, the water uptake can be described also as:



It is obvious that both of these processes are happened at the same time for the compositions with local distortion of the crystal lattice. Based on this, we can assume that in the structure of hydrated RP-compositions at least three different crystallographic positions of oxygen-hydrogen groups exist. Protons can be localized the structural oxygen atoms  $(\text{OH})_{\text{O}'}^{\bullet}$  and part of the oxygen-hydrogen groups may exist in the oxygen vacancies  $(\text{OH})_{\text{V}_o}^{\bullet}$  in the perovskite blocks and in the salt block in the interstitial oxygen positions  $(\text{OH})_{\text{i}}^{\bullet}$ .

Figure 6 represents the thermogravimetric (TG) data of hydrated compositions  $\text{BaLa}_2\text{In}_2\text{O}_7$  and  $\text{BaNd}_2\text{In}_2\text{O}_7$ . As we can see, three steps on the TG-curves for both compositions are observed. These results can be indirect evidence of the presence of oxygen vacancies in the structure of compositions  $\text{BaM}_2\text{In}_2\text{O}_7$ . The amount of water uptake is almost the same for both compositions and it is around 0.15–0.17 mol  $\text{H}_2\text{O}$  per formula  $\text{BaM}_2\text{In}_2\text{O}_7$  unit. Consequently, the difference between protonic conductivity values for the compositions  $\text{BaLa}_2\text{In}_2\text{O}_7$  and  $\text{BaNd}_2\text{In}_2\text{O}_7$  must be provided by the difference between protonic mobility only:

$$\sigma_i = z_i \cdot e \cdot \mu_i \cdot C_i \quad (5)$$

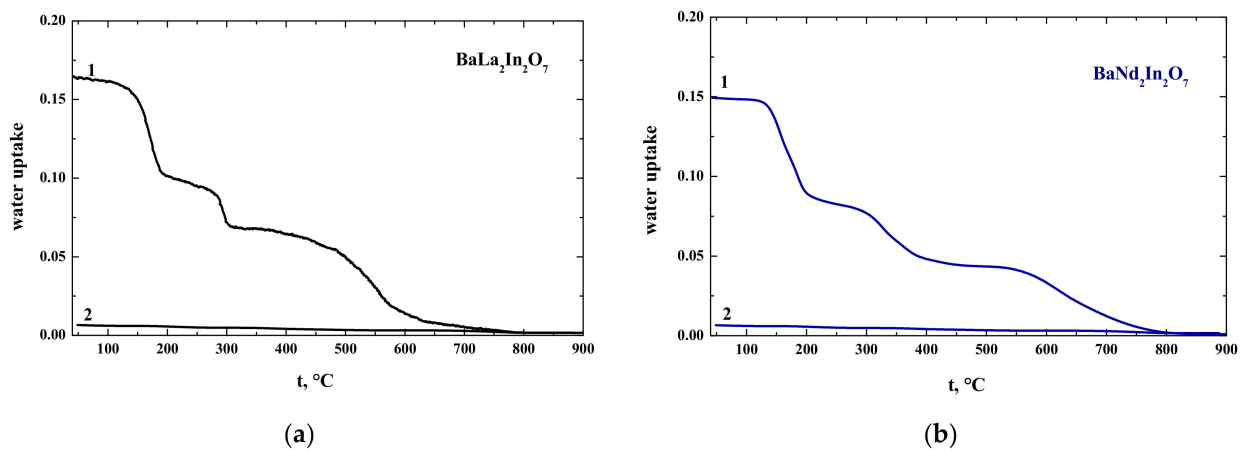


**Figure 6.** Thermogravimetry data for the  $\text{BaLa}_2\text{In}_2\text{O}_7$  (a) and  $\text{BaNd}_2\text{In}_2\text{O}_7$  (b) compounds obtained under wet (1) and dry (2) Ar.

The temperature dependencies of conductivity obtained under wet condition are presented in Figure 7a ( $p_{\text{H}_2\text{O}} = 2 \times 10^{-2}$  atm). The conductivity values for the composition  $\text{BaNd}_2\text{In}_2\text{O}_7$  are higher compared with the values for the composition  $\text{BaLa}_2\text{In}_2\text{O}_7$ . In the region of high temperatures ( $T > 700$  °C), where protonic transport is negligible, the conductivity values obtained under wet Ar are significantly lower than under wet air. In the region of low temperatures ( $T < 450$  °C), the conductivity values obtained under wet air and wet Ar are almost the same. In other words, the conductivity values obtained under wet air below 450 °C can be considered as the values of ionic conductivity. This statement is proved by the data obtained from the “ $\sigma$ - $p_{\text{O}_2}$ ” dependencies. As can be seen in Figure 8, the conductivity values obtained under wet condition and low temperatures ( $T < 450$  °C) are independent of the oxygen partial pressure even under oxidizing conditions ( $p_{\text{O}_2} = 10^{-5}$ –0.21 atm).

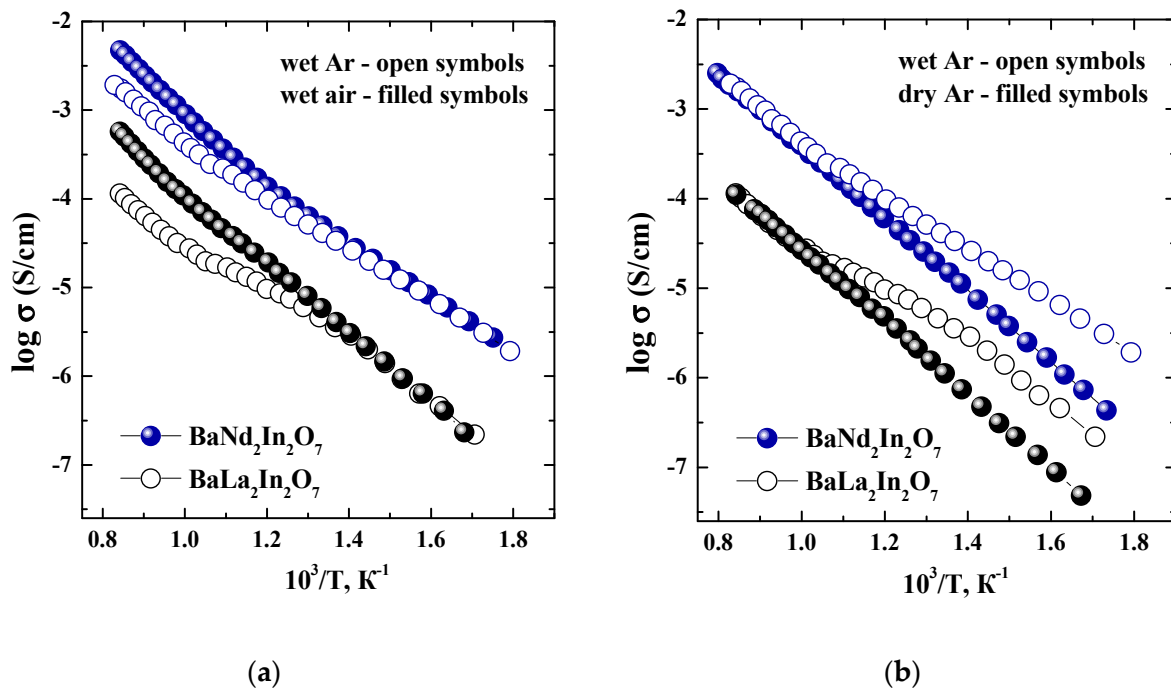


**Figure 7.** Temperature dependencies of conductivity for  $BaNd_2In_2O_7$  (blue symbols) and  $BaLa_2In_2O_7$  (black symbols) [17] obtained at wet Ar (open symbols) and wet air (filled symbols) (a); wet Ar (open symbols) and dry Ar (filled symbols) (b).

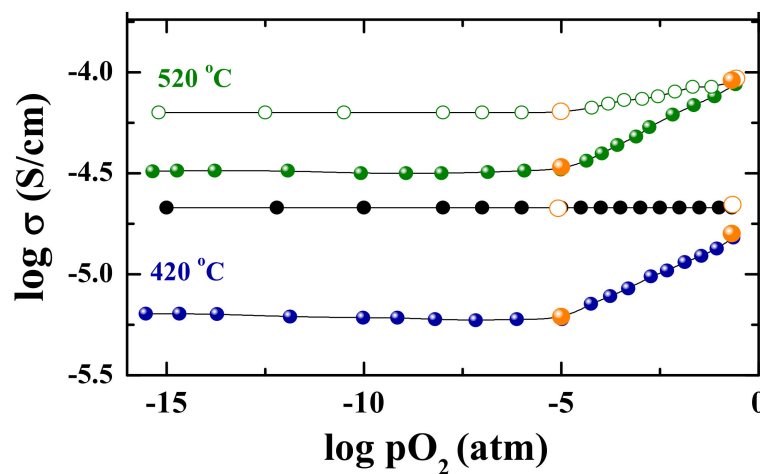


**Figure 8.** Oxygen partial pressure dependencies of the total conductivity for the  $BaNd_2In_2O_7$  sample at dry (filled symbols) and wet (open symbols) conditions and conductivity values from  $\sigma-10^3/T$  dependencies (orange symbols).

The effect of changes in the water partial pressure on the ionic conductivity is well visible in Figure 7b, where temperature dependencies of conductivity under dry and wet Ar are presented. As can be seen, the decrease in the temperature leads to the increase in the conductivity values obtained under wet Ar due to formation of the protonic charge carriers in the structure, which are more mobile in comparison with oxygen ions.

The protonic conductivity values were calculated as difference between the conductivity values in wet and dry Ar. The temperature dependencies of protonic conductivities for the compositions  $BaLa_2In_2O_7$  and  $BaNd_2In_2O_7$  are presented in Figure 9.

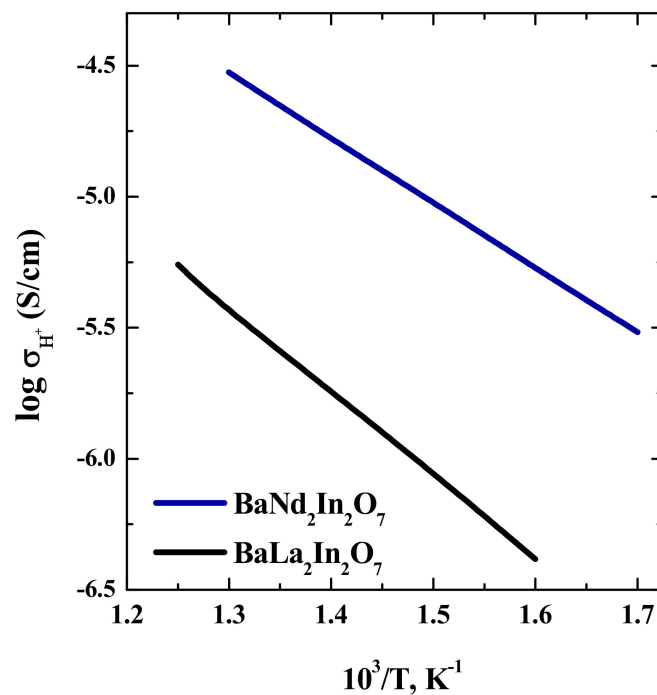


**Figure 9.** Temperature dependencies of protonic conductivity for  $BaNd_2In_2O_7$  (blue line) and  $BaLa_2In_2O_7$  (black line).

As can be seen, the values for  $BaNd_2In_2O_7$  are higher than for  $BaLa_2In_2O_7$  about one order of magnitude. The increase in the protonic conductivity values is well correlated with the decrease in the values of activation energy from 0.63 eV for  $BaLa_2In_2O_7$  to 0.5 eV for  $BaNd_2In_2O_7$ . Returning to the results of TG-measurements, which showed closeness of protons concentrations for both compositions, we can say, that the increase in the protonic conductivity values for the composition  $BaNd_2In_2O_7$  is due to the increase in the protons mobility. The calculation of protonic transport numbers  $t_H$  according to the formula:

$$t_H = \frac{\sigma_{H^+}}{\sigma_{wet\ air}} \quad (6)$$

This showed, that for both compositions  $BaLa_2In_2O_7$  and  $BaNd_2In_2O_7$  with decreasing temperature the increase in  $t_H$  occurs and the values reach up to 95% at the temperatures below 350 °C. Thus, these complex oxides can be considered as promising matrix compositions for creation of novel high-conductive protonic electrolytes with PR structure.

#### 4. Conclusions

In this paper, the complex oxides  $BaLa_2In_2O_7$  and  $BaNd_2In_2O_7$  were synthesized, and the local structure, water uptake, and the electrical conductivity were investigated. It was shown that the values of electrical conductivity of double-layered complex oxides with PR structure  $BaM_2In_2O_7$  ( $M = La, Nd$ ) are strongly depend on the nature of rare earth metal in the cationic sublattice. The change in the ionic radius of the element leads not only to the change in the unit cell parameters but also to the change in the local structure. It was shown that the composition  $BaNd_2In_2O_7$  is characterized by the higher values of electrical conductivity and the higher share of oxygen-ionic conductivity under dry air condition compared to the composition  $BaLa_2In_2O_7$ . The most likely reason for this is an increase in local distortions in the crystal lattice and the formation of a greater number of oxygen defects. Under wet air conditions both compositions are nearly pure protonic conductors below 350 °C.

**Author Contributions:** Conceptualization, I.A. and N.T.; methodology, I.A., D.M. and N.T.; investigation, A.G., K.B., E.A. and A.E.; data curation, N.T., K.B., E.A., A.E. and A.G.; writing—original

draft preparation, N.T.; writing—review and editing, N.T., I.A. and D.M. All authors have read and agreed to the published version of the manuscript.

**Funding:** This research was performed according to the budgetary plan of the Institute of High Temperature Electrochemistry and funded by the Budget of Russian Federation.

**Institutional Review Board Statement:** Not applicable.

**Informed Consent Statement:** Not applicable.

**Data Availability Statement:** Not applicable.

**Conflicts of Interest:** The authors declare no conflict of interest.

## References

1. Ruddlesden, S.N.; Popper, P. The compound  $\text{Sr}_3\text{Ti}_2\text{O}_7$  and its structure. *Acta Cryst.* **1958**, *11*, 54–55. [[CrossRef](#)]
2. Shimizu, K.; Tsuji, Y.; Hatamachi, T.; Toda, K.; Kodama, T.; Sato, M.; Kitayama, Y. Photocatalytic water splitting on hydrated layered perovskite tantalate  $\text{A}_2\text{SrTa}_2\text{O}_7 \cdot n\text{H}_2\text{O}$  (A = H, K, and Rb). *Phys. Chem. Chem. Phys.* **2004**, *6*, 1064–1069. [[CrossRef](#)]
3. Liang, Z.; Tang, K.; Shao, Q.; Lia, G.; Zeng, S.; Zheng, H. Synthesis, crystal structure, and photocatalytic activity of a new two-layer Ruddlesden–Popper phase,  $\text{Li}_2\text{CaTa}_2\text{O}_7$ . *J. Solid State Chem.* **2008**, *181*, 964–970. [[CrossRef](#)]
4. Wang, Y.; Wang, C.; Wang, L.; Hao, Q.; Zhu, X.; Chen, X.; Tang, K. Preparation of interlayer surface tailored protonated double-layered perovskite  $\text{H}_2\text{CaTa}_2\text{O}_7$  with n-alcohols, and their photocatalytic activity. *RSC Adv.* **2014**, *4*, 4047–4054. [[CrossRef](#)]
5. Wang, C.; Jin, Y.; Lv, Y.; Ju, G.; Chen, L.; Li, X.; Hu, Y. A bifunctional phosphor  $\text{Sr}_3\text{Sn}_2\text{O}_7:\text{Eu}^{3+}$ : Red luminescence and photochromism properties. *J. Lumin.* **2017**, *192*, 337–342. [[CrossRef](#)]
6. Zhang, L.; Sun, B.; Liu, Q.; Ding, N.; Yang, H.; Wang, L.; Zhang, Q. Novel layered perovskite  $\text{Sr}_3\text{Ti}_2\text{O}_7:\text{Eu}^{3+}$  phosphor with high-efficiency luminescence enhanced by charge compensation. *J. Alloys Compd.* **2016**, *657*, 27–31. [[CrossRef](#)]
7. Battle, P.D.; Rosseinsky, M.J. Synthesis, structure, and magnetic properties of n=2 Ruddlesden–Popper manganates. *Curr. Opin. Solid State Mater. Sci.* **1999**, *4*, 163–170. [[CrossRef](#)]
8. Ling, C.D.; Millburn, J.E.; Mitchell, J.F.; Argyriou, D.N.; Linton, J. Interplay of spin and orbital ordering in the layered colossal magnetoresistance manganite  $\text{La}_{2-2x}\text{Sr}_{1+2x}\text{Mn}_2\text{O}_7$  ( $0.5 \leq x \leq 1.0$ ). *Phys. Rev. B* **2000**, *62*, 15096–15111. [[CrossRef](#)]
9. Medvedeva, J.E.; Anisimov, V.I.; Mryasov, O.N.; Freeman, A.J. The role of Coulomb correlation in magnetic and transport properties of doped manganites:  $\text{La}_{0.5}\text{Sr}_{0.5}\text{MnO}_3$  and  $\text{LaSr}_2\text{Mn}_2\text{O}_7$ . *J. Phys. Condens. Matter* **2002**, *14*, 4533–4542. [[CrossRef](#)]
10. Taşarkuyu, E.; Coşkun, A.; Irmak, A.E.; Aktürk, S.; Ünlü, G.; Samancıoğlu, Y.; Yücel, A.; Sarıkürkçü, C.; Aksoy, S.; Acet, M. Effect of high temperature sintering on the structural and the magnetic properties of  $\text{La}_{1.4}\text{Ca}_{1.6}\text{Mn}_2\text{O}_7$ . *J. Alloys Compd.* **2011**, *509*, 3717–3722. [[CrossRef](#)]
11. Dudric, R.; Goga, F.; Neumann, M.; Mican, S.; Tetean, R. Magnetic properties and magnetocaloric effect in  $\text{La}_{1.4-x}\text{Ce}_x\text{Ca}_{1.6}\text{Mn}_2\text{O}_7$  perovskites synthesized by sol–gel method. *J. Mater. Sci.* **2012**, *47*, 3125–3130. [[CrossRef](#)]
12. Denbri, F.; Mahamdioua, N.; Meriche, F.; Altintas, S.P.; Terzioglu, C. Investigation of magneto-transport properties of the codoped  $\text{La}_{1.6-x}\text{Pr}_x\text{Ca}_{1.4-x}\text{Ba}_x\text{Mn}_2\text{O}_7$  ( $x = 0.2$  and  $0.4$ ) double-layered manganite. *J. Mater. Sci. Mater. Electron.* **2021**, *32*, 18808–18824. [[CrossRef](#)]
13. Boulahya, K.; Muñoz-Gil, D.; Gómez-Herrero, A.; Azcondo, M.T.; Amador, U.  $\text{Eu}_2\text{SrCo}_{1.5}\text{Fe}_{0.5}\text{O}_7$  a new promising Ruddlesden–Popper member as cathode component for intermediate temperature solid oxide fuel cells. *J. Mater. Chem. A* **2019**, *7*, 5601–5611. [[CrossRef](#)]
14. Wang, Q.; Hou, J.; Fan, Y.; Xi, X.; Li, J.; Lu, Y.; Huo, G.; Shao, L.; Fu, X.; Luo, J.  $\text{Pr}_2\text{BaNiMnO}_{7-\delta}$  double-layered Ruddlesden–Popper perovskite oxides as efficient cathode electrocatalysts for low temperature proton conducting solid oxide fuel cells. *J. Mater. Chem. A* **2020**, *8*, 7704–7712. [[CrossRef](#)]
15. Muñoz Gil, D.; Boulahya, K.; Santoyo, M.S.; Azcondo, M.T.; Amador, U. Superior Performance as Cathode Material for Intermediate-Temperature Solid Oxide Fuel Cells of the Ruddlesden–Popper n = 2 Member  $\text{Eu}_2\text{SrCo}_{0.50}\text{Fe}_{1.50}\text{O}_{7-\delta}$  with Low Cobalt Content. *Inorg. Chem.* **2021**, *60*, 3094–3105. [[CrossRef](#)]
16. Kananke-Gamage, C.C.W.; Ramezanipou, F. Variation of the electrocatalytic activity of isostructural oxides  $\text{Sr}_2\text{LaFeMnO}_7$  and  $\text{Sr}_2\text{LaCoMnO}_7$  for hydrogen and oxygen-evolution reactions. *Dalton Trans.* **2021**, *50*, 14196–14206. [[CrossRef](#)]
17. Tarasova, N.; Galisheva, A.; Animitsa, I.; Korona, D.; Kreimesh, H.; Fedorova, I. Protonic transport in layered perovskites  $\text{BaLa}_n\text{In}_n\text{O}_{3n+1}$  ( $n = 1, 2$ ) with Ruddlesden–Popper structure. *Appl. Sci.* **2022**, *12*, 4082. [[CrossRef](#)]
18. Kim, S.; Kim, G.; Manthiram, A. A review on infiltration techniques for energy conversion and storage devices: From fundamentals to applications. *Sustain. Energy Fuels* **2021**, *5*, 5024–503721. [[CrossRef](#)]
19. Klyndyuk, A.I.; Chizhova, E.A.; Kharytonau, D.S.; Medvedev, D.A. Layered oxygen-deficient double perovskites as promising cathode materials for solid oxide fuel cells. *Materials* **2022**, *15*, 141. [[CrossRef](#)]
20. Hanif, M.B.; Motola, M.; Qayyum, S.; Rauf, S.; Khalid, A.; Li, C.-J.; Li, C.-X. Recent advancements, doping strategies and the future perspective of perovskite-based solid oxide fuel cells for energy conversion. *Chem. Eng. J.* **2022**, *42815*, 132603. [[CrossRef](#)]
21. Shim, J.H. Ceramics breakthrough. *Nat. Energy* **2018**, *3*, 168–169. [[CrossRef](#)]

22. Meng, Y.; Gao, J.; Zhao, Z.; Amoroso, J.; Tong, J.; Brinkman, K.S. Review: Recent progress in low-temperature proton-conducting ceramics. *J. Mater. Sci.* **2019**, *54*, 9291–9312. [[CrossRef](#)]
23. Kim, J.; Sengodan, S.; Kim, S.; Kwon, O.; Bud, Y.; Kim, G. Proton conducting oxides: A review of materials and applications for renewable energy conversion and storage. *Renew. Sustain. Energy Rev.* **2019**, *109*, 606–618. [[CrossRef](#)]
24. Medvedev, D.A. Current drawbacks of proton-conducting ceramic materials: How to overcome them for real electrochemical purposes. *Curr. Opin. Green Sustain. Chem.* **2021**, *32*, 100549. [[CrossRef](#)]
25. Bello, I.T.; Zhai, S.; He, Q.; Cheng, C.; Dai, Y.; Chen, B.; Zhang, Y.; Ni, M. Materials development and prospective for protonic ceramic fuel cells. *Int. J. Energy Res.* **2022**, *46*, 2212–2240. [[CrossRef](#)]
26. Irvine, J. Roadmap on inorganic perovskites for energy applications. *J. Phys. Energy* **2021**, *3*, 031502. [[CrossRef](#)]
27. Titov, Y.A.; Belyavina, N.M.; Markiv, V.Y.; Slobodyanik, M.S.; Krayevska, Y.A.; Yaschuk, V.P. Synthesis and crystal structure of  $\text{BaLn}_2\text{In}_2\text{O}_7$ . *Rep. Natl. Acad. Sci. Ukr.* **2010**, *1*, 148–153.
28. Caldes, M.; Michel, C.; Rouillon, T.; Hervieu, M.; Raveau, B. Novel indates  $\text{Ln}_2\text{BaIn}_2\text{O}_7$ ,  $n = 2$  members of the Ruddlesden–Popper family ( $\text{Ln} = \text{La}, \text{Nd}$ ). *J. Mater. Chem.* **2002**, *12*, 473–476. [[CrossRef](#)]
29. Fujii, K.; Esaki, Y.; Omoto, K.; Yashima, M.; Hoshikawa, A.; Ishigaki, T.; Hester, J.R. New Perovskite-Related Structure Family of Oxide-Ion Conducting Materials  $\text{NdBaInO}_4$ . *Chem. Mater.* **2014**, *26*, 2488–2491. [[CrossRef](#)]
30. Fujii, K.; Shiraiwa, M.; Esaki, Y.; Yashima, M.; Kim, S.J.; Lee, S. Improved oxide-ion conductivity of  $\text{NdBaInO}_4$  by Sr doping. *J. Mater. Chem. A* **2015**, *3*, 11985. [[CrossRef](#)]
31. Ishihara, T.; Yan, Y.; Sakai, T.; Ida, S. Oxide ion conductivity in doped  $\text{NdBaInO}_4$ . *Solid State Ionics* **2016**, *288*, 262–265. [[CrossRef](#)]
32. Yang, X.; Liu, S.; Lu, F.; Xu, J.; Kuang, X. Acceptor Doping and Oxygen Vacancy Migration in Layered Perovskite  $\text{NdBaInO}_4$ -Based Mixed Conductors. *J. Phys. Chem. C* **2016**, *120*, 6416–6426. [[CrossRef](#)]
33. Fijii, K.; Yashima, M. Discovery and development of  $\text{BaNdInO}_4$ —A brief review. *J. Ceram. Soc. Jpn.* **2018**, *126*, 852–859. [[CrossRef](#)]
34. Zhou, Y.; Shiraiwa, M.; Nagao, M.; Fujii, K.; Tanaka, I.; Yashima, M.; Baque, L.; Basbus, J.F.; Moggi, L.V.; Skinner, S.J. Protonic Conduction in the  $\text{BaNdInO}_4$  Structure Achieved by Acceptor Doping. *Chem. Mater.* **2021**, *33*, 2139–2146. [[CrossRef](#)]
35. Tarasova, N.; Galisheva, A.; Animitsa, I.  $\text{Ba}^{2+}/\text{Ti}^{4+}$ -co-doped layered perovskite  $\text{BaLaInO}_4$ : The structure and ionic ( $\text{O}^{2-}$ ,  $\text{H}^+$ ) conductivity. *Int. J. Hydrogen Energy* **2021**, *46*, 16868–16877. [[CrossRef](#)]
36. Tarasova, N.A.; Galisheva, A.O.; Animitsa, I.E.; Lebedeva, E.L. Oxygen-Ion and Proton Transport in Sc-Doped Layered Perovskite  $\text{BaLaInO}_4$ . *Russ. J. Electrochem.* **2021**, *57*, 1008–1014. [[CrossRef](#)]
37. Tarasova, N.A.; Galisheva, A.O.; Animitsa, I.E.; Dmitrieva, A.A. The Effect of Donor Doping on the Ionic ( $\text{O}^{2-}$ ,  $\text{H}^+$ ) Transport in Novel Complex Oxides  $\text{BaLaIn}_{1-x}\text{Nb}_x\text{O}_{4+x}$  with the Ruddlesden–Popper Structure. *Russ. J. Electrochem.* **2021**, *57*, 962–969. [[CrossRef](#)]
38. Tarasova, N.; Animitsa, I.; Galisheva, A. Effect of acceptor and donor doping on the state of protons in block-layered structures based on  $\text{BaLaInO}_4$ . *Solid State Commun.* **2021**, *323*, 14093. [[CrossRef](#)]
39. Tarasova, N.; Animitsa, I.; Galisheva, A. Spectroscopic and transport properties of Ba- and Ti-doped  $\text{BaLaInO}_4$ . *J. Raman Spec.* **2021**, *52*, 980–987. [[CrossRef](#)]
40. Tarasova, N.; Animitsa, I.; Galisheva, A. Effect of doping on the local structure of new block-layered proton conductors based on  $\text{BaLaInO}_4$ . *J. Raman Spec.* **2021**, *51*, 2290–2297. [[CrossRef](#)]
41. Tarasova, N.; Animitsa, I. Materials  $\text{A}^{\text{II}}\text{LnInO}_4$  with Ruddlesden–Popper structure for electrochemical applications: Relationship between ion (oxygen-ion, proton) conductivity, water uptake and structural changes. *Materials* **2022**, *15*, 114. [[CrossRef](#)] [[PubMed](#)]
42. Scherban, T.; Villeneuve, R.; Abello, L.; Lucazeau, G. Raman scattering study of acceptor-doped  $\text{BaCeO}_3$ . *Solid State Ion.* **1993**, *61*, 93–98. [[CrossRef](#)]
43. Chemarin, C.; Rosman, N.; Pagnier, T.; Lucazeau, G. High-Pressure Raman Study of Mixed Perovskites  $\text{BaCe}_x\text{Zr}_{1-x}\text{O}_3$  ( $0 \leq x \leq 1$ ). *J. Solid State Chem.* **2000**, *149*, 298–307. [[CrossRef](#)]
44. Paul, B.; Chatterjee, S.; Gop, S.; Roy, A.; Grover, V.; Shukla, R.; Tyagi, A.K. Evolution of lattice dynamics in ferroelectric hexagonal  $\text{REInO}_3$  ( $\text{RE} = \text{Ho}, \text{Dy}, \text{Tb}, \text{Gd}, \text{Eu}, \text{Sm}$ ) perovskites. *Mater. Res. Express* **2016**, *3*, 075703. [[CrossRef](#)]
45. Kamba, S.; SamoukPina, F.; Kadlec, F.; Pokorný, J.; Petzelt, J.; Reaney, I.M.; Wise, P.L. Composition dependence of the lattice vibrations in  $\text{Sr}_{n+1}\text{Ti}_n\text{O}_{3n+1}$  Ruddlesden–Popper homologous series. *J. Eur. Ceram. Soc.* **2003**, *23*, 2639–2645. [[CrossRef](#)]
46. Iliev, M.N.; Popov, V.N.; Litvinchuk, A.P.; Abrashev, M.V.; Backstrom, J.; Sun, Y.Y.; Mena, R.L.; Chu, C.W. Comparative Raman studies of  $\text{Sr}_2\text{RuO}_4$ ,  $\text{Sr}_3\text{Ru}_2\text{O}_7$  and  $\text{Sr}_4\text{Ru}_3\text{O}_{10}$ . *Physica B* **2005**, *358*, 138–152. [[CrossRef](#)]
47. Shannon, R.D. Revised effective ionic radii and systematic studies of interatomic distances in halides and chalcogenides. *Acta Cryst.* **1976**, *A32*, 751–767. [[CrossRef](#)]